Journal of Solid State Chemistry 184 (2011) 2478–2484

Contents lists available at ScienceDirect

Journal of Solid State Chemistry

journal homepage: www.elsevier.com/locate/jssc

Selective synthesis of boron nitride nanotubes by self-propagation high-temperature synthesis and annealing process

Jilin Wang [a], Laiping Zhang [a], Guowei Zhao [a], Yunle Gu [a,b,*], Zhanhui Zhang [a,b], Fang Zhang [a,b], Weimin Wang [c]

[a] School of Materials Science and Engineering, Wuhan Institute of Technology, Wuhan 430073, China
[b] Nano and Ceramic Materials Research Center, Wuhan Institute of Technology, Wuhan 430073, China
[c] The State Key Laboratory of Advanced Technology for Materials Synthesis and Processing, Wuhan University of Technology, Wuhan 430073, China

ARTICLE INFO

Article history:
Received 23 April 2011
Received in revised form
13 July 2011
Accepted 17 July 2011
Available online 22 July 2011

Keywords:
Boron nitrides
Nanotubes
Chemical vapor deposition
Synthesis

ABSTRACT

Four types of BN nanotubes are selectively synthesized by annealing porous precursor in flowing NH_3 and NH_3/H_2 atmosphere at temperature ranging from 1000 to 1200 °C in a vertical furnace. The as-synthesized BN nanotubes, including cylinder, wave-like, bamboo-like and bubble-chain, are characterized by XRD, FTIR, Raman, SEM, TEM and HRTEM. Three phenomenological growth models are proposed to interpret growth scenario and structure features of the four types of BN nanotubes. Selectivity of nanotubes formation is estimated as approximately 80–95%. The precursor containing B, Mg, Fe and O prepared by self-propagation high-temperature synthesis (SHS) method plays a key role in selective synthesis of the as-synthesized BN nanotubes. Chemical reactions are also discussed.

1. Introduction

Since boron nitride (BN) nanotubes were first produced using plasma discharge [1], various synthesis techniques have been developed. The methods can be roughly classified in four categories as physical method, chemical vapor deposition (CVD), chemical synthesis and hard template methods. Physical methods have the common feature of using high temperature normally above 2000 °C by rapid energy input with physical means such as arc-discharge, laser ablation and evaporation. Chemical synthesis methods produce BN nanotubes through chemical reactions usually confined in sealed autoclaves heated at lower temperature below 800 °C under high self-generated pressure. Hard template methods convert carbon nanotubes to BN nanotubes, or employ porous silica and anodic aluminum oxide (AAO) as templates [2,3].

In contrast, in the CVD process, as well as in most physical and chemical synthesis, the growth of BN nanotubes inherently associates with in-situ formed soft templates such as reactive liquid droplets and catalyst particles. The most accepted theory for the growth of BN-nanotubes is the vapor–liquid–solid (VLS) mechanism [4]. A CVD process can operate at a relatively low temperature ranging from 600 to 1300 °C and under normal or lower pressure [5]. In addition, the characteristics of BN nanotubes including types, diameter, length, wall thickness, defects, chirality and configuration can be well controlled.

Various boron-containing precursors can be used for preparing films and/or powders of BN nanotubes by CVD method. For example, gaseous boron-containing precursors can be employed including diborane (B_2H_6) [6,7], borazine ($B_3N_3H_6$) [8,9] and trimethyl borate ($C_3H_9BO_3$) [10], while solid boron-containing precursors can be elemental boron [11–18], iron boride (FeB) [19,20], B_2O_3 [21], boric acid (H_3BO_3) [22] and $Ba(BO_2)_2$ [23]. However, the VLS mechanism implies that nanotube diameters are related to the sizes of catalyst particles. Therefore, high dispersion and homogeneity of catalyst in solid precursor is crucial for synthesis of uniform BN nanotubes. Many researchers have resorted to extensive ball-milling for dispersing catalyst before subsequent annealing process. For example, a variety types of BN nanotubes can be successfully synthesized by the ball-milling-annealing method from elemental boron [24–28] and boron nitride [29,30].

In this article, we report selective synthesis of four types of BN nanotubes using a porous precursor prepared by self-propagation high-temperature synthesis (SHS). The SHS method is a novel technology for obtaining precursor with high dispersion and homogeneity of catalyst. And the porous precursor plays an important role in bulk synthesis process. A scaled-up batch production of four types of BN nanotubes with high yields and good quality is demonstrated. Three phenomenological growth

* Corresponding author at: School of Materials Science and Engineering, Wuhan Institute of Technology, Nano and Ceramic Materials Research, XiongChu Str. 693, Wuhan, China. Fax: +86 27 8719 3199.
E-mail address: ncm@mail.wit.edu.cn (Y. Gu).

0022-4596/$ - see front matter © 2011 Elsevier Inc. All rights reserved.
doi:10.1016/j.jssc.2011.07.026

models, i.e. base, tip and base-tip (including based tip) growth mechanism, will be proposed to reveal growth scenario and characteristics of the as-synthesized BN nanotubes.

2. Experimental section

The porous precursors can be prepared by the SHS method through reacting B_2O_3 and Mg in the presence of addictives including boron-containing diluents and/or catalysts, such as Fe_2O_3 and FeB, The reagents B_2O_3, Mg and Fe_2O_3 were all of analytical pure grade and of about 150–300 mesh powders. The FeB was of 200 mesh commercial powders and had a boron content around 16.20 wt%.

In this article, the porous precursor $B_{31}Fe_{17}(MgO)_{27}$ was employed for selective synthesis of four types of BN nanotubes. In a typical experimental procedure, the porous precursor $B_{31}Fe_{17}(MgO)_{27}$ was prepared by SHS method from 3.60 kg B_2O_3, 4.25 kg Mg, 1.10 kg Fe_2O_3 and 6.50 kg FeB. Firstly, the raw material powders were mixed thoroughly by a blender mixer for about 10–20 min. Then, the mixture were placed in a SHS reactor and ignited by heating to the temperature ranging from 700 to 800 °C for 5–15 min in an argon atmosphere. After combustion, about 15.30 kg porous precursor $B_{31}Fe_{17}(MgO)_{27}$ was prepared. The porous precursor around 3.8 kg was crashed into debris and placed into the alumina tube of about 80 cm in diameter and some 5 mm in thickness in a vertical annealing furnace. About 50 mesh woven sheets of about 70 cm in diameter made of fine iron wires were placed uniformly between precursor debris. The furnace was heated to temperatures in the range from 1000 to 1200 °C at a rate of 7 °C min^{-1} and maintained for 6–12 h. The flow rates of NH_3 or NH_3/N_2 atmospheres were regulated ranging from 0.5 to 10 L min^{-1} by a circulation pump.

After the furnace cooled to room temperature naturally, about 40 g of white BN nanotubes ($BN_{NT}1$) were collected from surface deposition of the iron woven sheets by ultrasonication in a 0.5 M HCl solution followed by filtration, washing with distilled water and drying at 80°C in vacuum. The BN nanotube purity of $BN_{NT}1$ was of above 90 wt%.

In addition, about 1 kg BN nanotube powders ($BN_{NT}2$) was obtained by purifying the annealed precursor powders by dispersing in 5 M hydrochloric acid and stirred at 60 °C at least 24 h followed by filtration and washing with 1 M nitric acid at ambient temperature. The BN nanotube purity of $BN_{NT}2$ was of normally around 80 wt%.

The yields of $BN_{NT}1$ were rather low, only less than 5 wt% of the total yields of BN nanotubes. Both $BN_{NT}1$ and $BN_{NT}2$ had similar structural features, and can be easily dispersed in anhydrous ethanol by ultrasonication.

The as-synthesized BN nanotubes were characterized by X-ray powder diffraction (XRD) using a Shimadzu XD-5A X-ray diffractometer or a RiGaKu D/MAX-IIIA X-ray diffractometer with Cu$K\alpha$ radiation (wavelength $\lambda=1.5406$ Å). Raman spectra were recorded at room temperature on a Nicolet DXR Raman spectrometer using Nd:YAG laser at an excitation of 532 nm. Fourier transform infrared (FTIR) spectra were recorded on a Nicolet 6700 Fourier transform infrared spectrometer in transmission mode using a KBr wafer. The scanning electron microscopy (SEM) and energy dispersive X-ray spectra (EDX) were studied using a Hitachi S-3400N scanning electron microscope. The field emission scanning electron microscopy (FSEM) was on a Hitachi S-4800 or a FEI Sirion 200 field emission scanning electron microscope. Samples were observed by spreading on a conductive tape spattered with Au or Pt. Transmission electron microscopy (TEM) and high-resolution transmission electron microscopy (HRTEM) were studied on a JEOL JEM-2100F or a JEOL JEM-2100 transmission electron microscope. Samples were ultrasonically dispersed in ethanol and deposited on copper grids coated with amorphous or holey carbon films.

3. Results and discussion

$B_{31}Fe_{17}(MgO)_{27}$ was only stands for the mixed chemical elements in the precursor prepared by SHS reaction using Mg, B_2O_3, Fe_2O_3 and FeB as the starting materials. Fig. 1 shows the typical SEM, TEM and HRTEM images of the as-grown BN nanotubes. These nanotubes are the so-called cylinder, wave-like, bamboo-like and bubble-chain, respectively. Annealing condition and the characteristics of these BN nanotubes are listed in Table 1.

The four type as-synthesized BN nanotubes are different from one another meanly by internal structures. Both cylinder (Fig. 1a3) and wave-like BN nanotubes (Fig. 1b3) have a hollow core along the center of the nanotubes from one end to the other. The cylinder has smooth internal walls and do not have inside BN structures (Fig. 1a2), while the wave have wave-like internal BN layers (Fig. 1b2). Unlike the wave-like structures of a grass that surround a stem, the wave-like tubes have many leaves inside the tubes surrounding internal walls. Nevertheless these two types have similar appearance and cannot be clearly differentiated only by their SEM (Fig. 1a1) and FSEM (Fig. 1b1) images.

The other two types of BN nanotubes, the bamboo-like (Fig. 1c3) and the bubble-chain (Fig. 1d3) BN nanotubes, have the same feature of obstructed internal structures. Unlike the bamboo-like BN nanotubes (Fig. 1c2), bubble-chain BN nanotubes (Fig. 1d2) are very weakly interconnected. The interconnections of bamboo-like segments are much stronger because they have more wide-span cross-segment BN layers in outerwalls. Bubble-chains have cross-segment BN layers only adjacently connected just like chains. These two types have somewhat different looks and can be roughly differentiated from the FSEM images (Fig. 1c1and 1d1).

The characterization of a cylindrical BN nanotube by SEM, TEM and HRTEM is shown in Fig. 1a1–a3. The SEM image shows that the as-synthesized BN nanotubes have an average length of more than 10 μm with a diameter of 30–300 nm. The cylinder tube in Fig. 1a2 has a multi-walled structure with a diameter about 150 nm. Its wall thickness can be determined as about 17 nm (Fig. 1a3). The HRTEM image inserted in Fig. 1a3 indicates a well-crystallized wall structure by the clear fringes with an interplanar distance of 0.34 nm, which corresponds to the d_{002} spacing of the hexagonal phase of BN. The composition of the sample was also studied by energy dispersive X-ray spectra (EDX). Strong signals of boron and nitrogen were detected. Quantitative analyses indicated that the molar ratio of B:N was 1:1.052, close to that of BN. The total BN contents of the four types of $BN_{NT}1$ and $BN_{NT}2$ samples were all above 95 wt%. The impurities were mainly surface oxygen and small amount of catalyst element Fe and Mg.

The sample of the as-synthesized cylindrical BN nanotubes were also characterized by X-ray powder diffraction (XRD), Raman and Fourier transform infrared (FTIR) spectroscopy. As shown in Fig. 2a, the XRD pattern revealed five peaks at d-spacings of 3.336, 2.165, 2.063, 1.664 and 1.253 Å, that can be indexed as the (002), (100), (101), (004) and (100) planes of hexagonal phase of BN. The lattice constants were $a=2.504$ and $c=6.668$ Å, which is close to the values $a=2.503$ and $c=6.661$ Å in JCPDF card No. 73-2095. The Raman spectrum (Fig. 2b) shows a sharp peak at 1360 cm^{-1}, corresponding to the E_{2g} in-plane vibration mode of the hexagonal BN networks. Similar result was also reported previously by Lee et al. [17]. The weak peak at about 780 cm^{-1} in the Raman spectrum is due to the glass holder

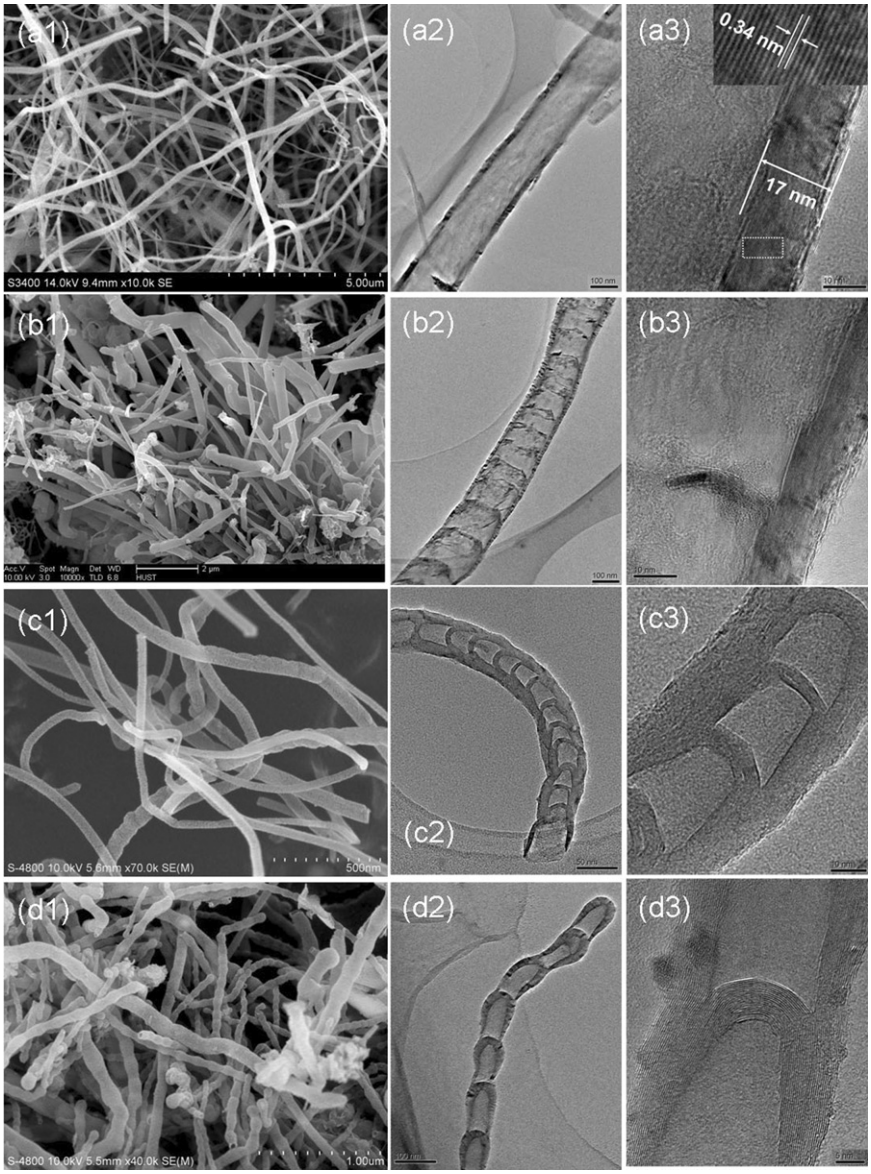

Fig. 1. Typical SEM and FSEM (1), TEM (2) and HRTEM (3) images of the as-grown four types of BN nanotubes prepared by annealing porous precursor $B_{31}Fe_{17}(MgO)_{27}$: (a) cylindrical BN nanotubes, (b) wave-like BN nanotubes, (c) bamboo-like BN nanotubes and (d) bubble-chain BN nanotubes. Scale bars: (a1) 5 μm, (a2) 100 nm, (a3) 10 nm, (b1) 2 μm, (b2), 100 nm, (b3), 10 nm, (c1), 500 nm, (c2) 50 nm, (c3) 10 nm, (d1) 1 μm, (d2) 100 nm and (d3) 5 nm.

used during the analysis. The wide-scan FTIR spectrum in the range of 500–4000 cm^{-1} is shown in Fig. 2c. Two absorption bands of hexagonal phase of BN show at 800 and 1380 cm^{-1} due to the characteristic vibrations of the R-mode (moving radially in ward or outward the plane) and the L-mode (in-plane stretching along the longitudinal or tube axis), respectively. The shoulder peak at 1530 cm^{-1} is due to the stretching of the hexagonal BN network along the tangential directions (T-mode), which is the characteristic absorption of well-crystallized BN nanotubes. A peak at about 1130 cm^{-1} emerges in the deconvolution spectrum (Fig. 2d) of the main peak around 1380 cm^{-1}. It can be assigned to vibrations like those of wurtzite BN presumablely for structure defects in the as-grown cylinder type of BN nanotubes:

$$8B_2O_3 + 27Mg + Fe_2O_3 + 15FeB = B_{31}Fe_{17}(MgO)_{27} \quad (1)$$

$$B_{31}Fe_{17}(MgO)_{27} + 31NH_3 = 31B^* + 31N^* + Fe_{17}(MgO)_{27} + 93/2H_2 \quad (2)$$

$$39/2H_2 + 13/2N_2 = 13NH_3 \quad (3)$$

$$x(B^* + N^*) + Fe_{17}(MgO)_{27} = xBN_{NT} + 17Fe + 27MgO \quad (4)$$

$$(31-x)(B^* + N^*) = (31-x)BN_{FL}(x = 0-31, \text{ NT} = \text{nanotubes, FL} = \text{non-tubular BN}) \quad (5)$$

The chemical reaction mechanism for the formation of the as-synthesized BN nanotubes can be described in Eqs. (1)–(5). As shown in Eq. (1), the porous precursor $B_{31}Fe_{17}(MgO)_{27}$ was made by SHS process from B_2O_3 and Mg using FeB and Fe_2O_3 as the additives. The SHS synthesis generally resulted in very high yields above 95 wt%, so the chemical composition formula of the SHS products can be expressed approximately as $B_{31}Fe_{17}(MgO)_{27}$. However, the phase composition was very complicated. This porous concrete material can be generally defined as boron-catalyst-containing particles dispersed on MgO particles. During the annealing process, boron-catalyst-containing species, such as iron boride, magnesium borides, boron sub-oxides and FeO reacted with NH_3 and produced nascent boron (B^*) and nitrogen

(N^*) vapor as in Eq. (2). Liquid droplets of catalyst Fe or Fe–Mg alloy supported on MgO particles, expressed as $Fe_{17}(MgO)_{27}$ can be simultaneously in-situ generated from metal borides and oxides. Reduction reactions may take place preferably by reacting iron oxides and boron sub-oxides with NH_3, especially when N_2 gas was added into the vapor stream, which can react with hydrogen reproducing NH_3 in the presence of ion catalyst as in Eq. (3). According to the catalytic VLS growth mechanism [4], BN nanotubes can be grown from the B* and N* vapor by the catalytic VLS growth mechanism with the assistance of in-situ formed liquid catalyst droplets as in Eq. (4). Small amount of non-tubular forms of hexagonal BN, preferably BN flakes, may also be produced simultaneously as a rival growth process through a vapor–solid (VS) growth mechanism due to the lack of catalyst. Therefore, the selectivity of BN nanotubes can be expressed as $x/31$ according to Eqs. (4) and (5), where the value of x was experimentally estimated as approximately 25–30 according to the selectivity of the as-synthesized BN nanotubes.

A literature survey reveals various base (root) and tip growth models have been suggested for understanding the growth mechanism of some specific types of nanotubes [19,30–32]. Furthermore, Helveg et al. [33] have shown in-situ based tip growth TEM images of a carbon nanotube, where the catalyst droplet was pulled up from the substrate completely to form a tip. Taking whichever growth models, catalyst drop is the only growing point of BN nanotubes according to the VLS growth mechanism.

We propose three growth models for all types of BN nanotubes and schematically illustrated in Fig. 3. For each type of BN nanotubes, the growth points can be at either base, or tip, or both base and tip catalyst drops, which depend on many factors. The strength of the interaction between catalyst and base or BN

Table 1
Annealing condition and the characteristics of the four types of as-synthesized BN nanotubes.

Types of BN nanotubes	Cylinder	Wave-like	Bamboo-like	Bubble-chain
Annealing condition[a]				
Flowing atmosphere	NH_3	NH_3	NH_3	NH_3/N_2=3:1 v/v
Flow rate (L min^{-1})	0.5–10	0.5–10	0.5–10	0.5–10
Temperature (°C)	1085	1165	1150	1180
Annealing time (h)	12	8	10	6
Yields and purity[b]				
$BN_{NT}1$ content (wt%)	≥95	≥95	≥90	≥90
$BN_{NT}2$ content (wt%)	≥85	≥85	≥80	≥80
Total BN content (wt%)	97.1	96.5	96.1	95.4
Characteristics of BN nanotubes[c]				
Diameter mean (nm)	100	150	50	80
Length mean (μm)	≥10	≥5	≥5	≥5

[a] The porous precursor $B_{31}Fe_{17}(MgO)_{27}$ was prepared by SHS method from B_2O_3, Mg, FeB and Fe_2O_3 as described in the experimental procedure. Flow rates were tuned within the range of 0.5–10 L/min by a circulation pump. The range listed here is merely scopes without optimization.

[b] $BN_{NT}1$ and $BN_{NT}2$ were obtained by different collecting and purifying methods as described in the experimental procedure. Total BN contents were the results from quantitative analyses by EDX spectra.

[c] Nanotube contents, (outside) diameter, internal diameter and nanotube length were approximately estimated according to the statistical analyses by TEM and SEM microscopies.

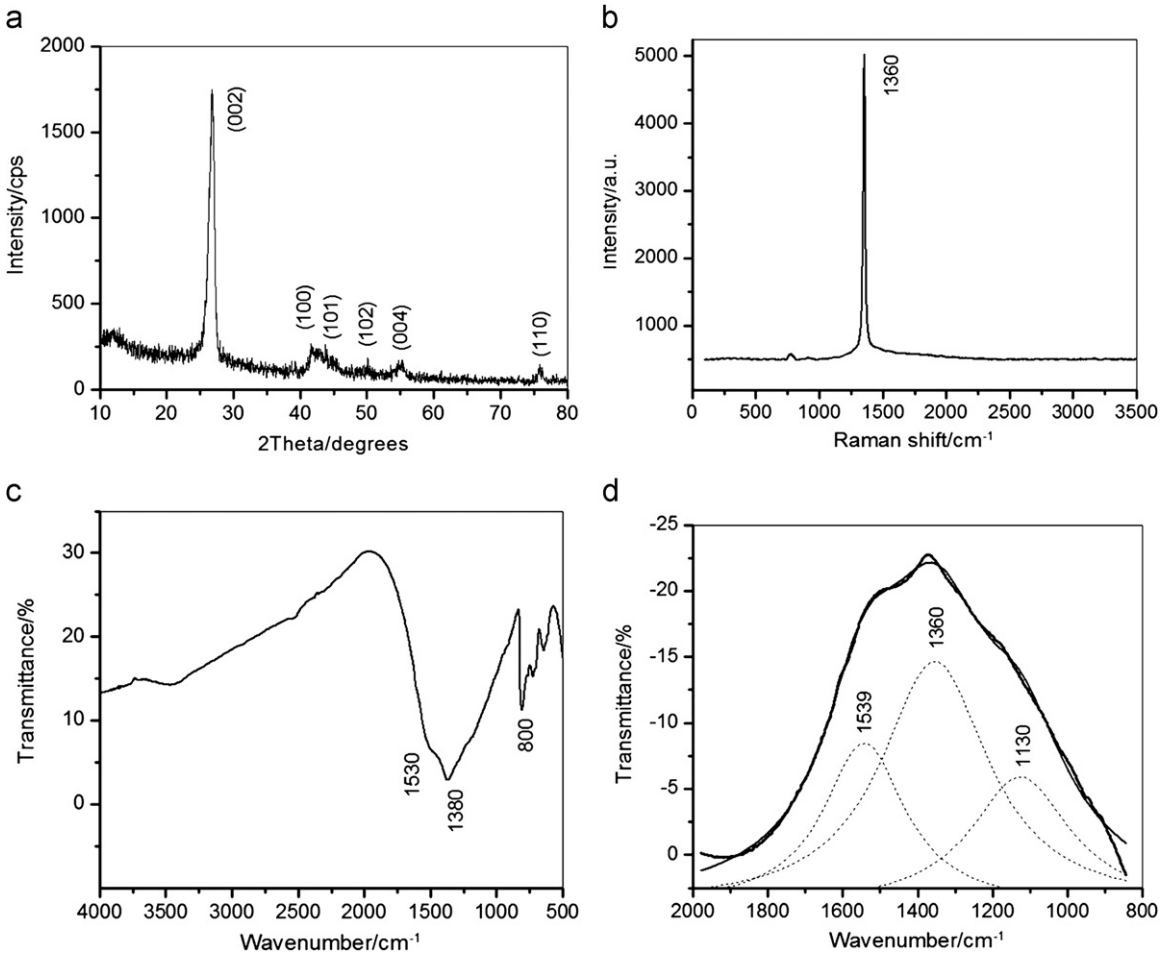

Fig. 2. The XRD pattern (a), Raman spectrum (b), wide-scan FTIR spectrum (c) and the deconvolution FTIR spectrum (d) of the as-synthesized BN nanotubes.

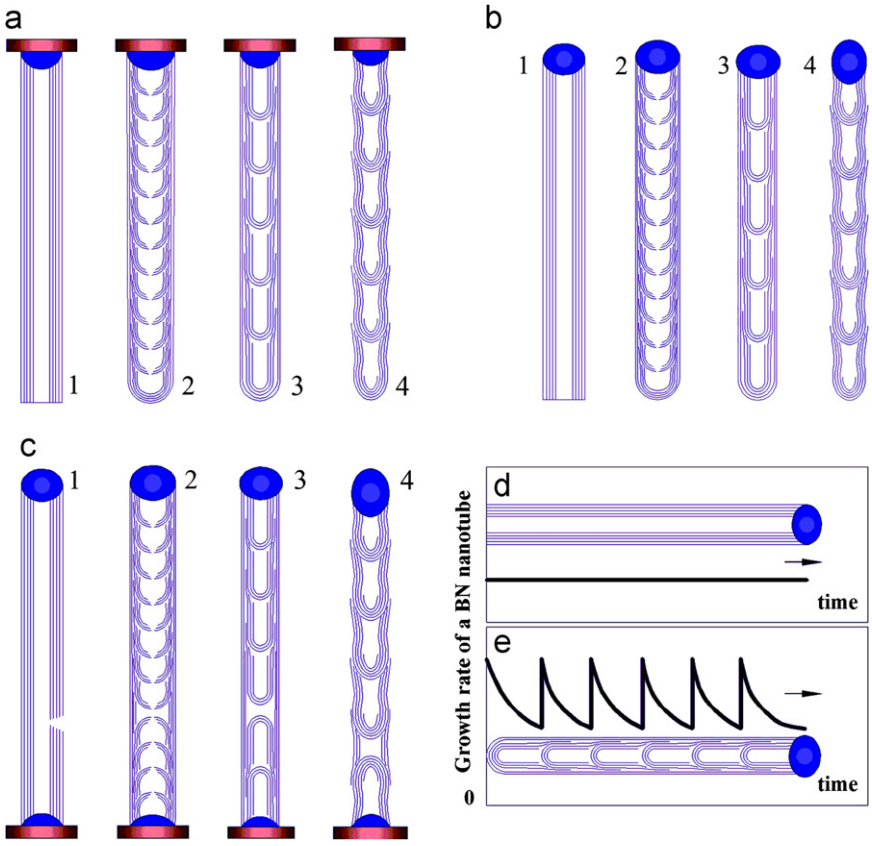

Fig. 3. Schematic illustrations of three growth models and the corresponding features of growth rates. Growth models: (a) base growth, (b) tip growth and (c) base-tip growth (including based tip growth): (1) cylinder, (2) wave-like, (3) bamboo-like and (4) bubble-chain. Growth rates: (d) cylinder and (e) bamboo-like BN nanotubes. The arrows denote the movement direction of the tip catalyst droplets.

layers is the key factor. Therefore, there are three growth models, the so-called base growth (Fig. 3a), tip growth (Fig. 3b) and base-tip growth (Fig. 3c). In particular, there have to be an initial open tip (Fig. 3a1 and b1) or a hole (Fig. 3c1) for the cylinder type models. In the base-tip growth model, catalyst drop may not exist at the base roots when the initial drop is completely drawn away to the tip. The base-tip growth model without base catalyst is very similar to the tip growth model, but they are different models because the BN nanotube is fixed on substrate for the base-tip growth, while the starting growing point for the tip growth is completely independent. The former has two growing points and the later has only one. In strict sense, base-tip growth without base catalyst is actually based tip growth as previously observed by Helveg et al. [33].

In principle, the four types of BN nanotubes can be simply classified in two categories by growth rate. The growth rate is the velocity of bottom-up self-assembly of boron (B^*) and nitrogen (N^*) atoms into a BN nanotube, which is closely associated with vapor condition, annealing parameters and in-situ formed catalyst. Changing of growth rates may occur due to the variations of vapor concentration, local temperature and reshaping of certain liquid catalyst droplets. The instantaneous growth rate can be defined as the partial derivative relations of BN nanotube volume with respect to time. In order to grow a cylinder BN nanotube, the growth rate should be either constant or smoothly changing. For other three types that have internal BN structures including wave-like (Fig. 3a2, b2 and c2), bamboo-like (Fig. 3a3, b3 and c3) and bubble-chain (Fig. 3a4, b4 and c4), the grown rates should be only abruptly changing.

We explain the abruptly changing of growth rates by a pressure-induced mutation mechanism, which is somewhat similar to the capillary mechanism previously proposed by Chadderton and Chen [32]. Abruptly changing of growth rates may occur simultaneously along with the repeatedly shutting and opening of the internal space of the nanotube confined by the wall of BN nanotube and catalyst droplet surface, or participated by the root base. Unlike cylinder BN nanotubes, these internal-structured nanotubes do not have invariable channels from inside to outside of the internal space during the growth process. For example, starting the growth process with a locked state, increase in internal void will strengthen the backward force applying to the forward-moving droplet. The forward driving force is self-generated by newly formed BN layers on the outside surface of the droplet. This driving force will be counteracted gradually and even be converted to a backward driving force by the resistance of negative internal pressure. An aperture will suddenly burst when the liquid–solid interface cannot withstand the shearing stress due to the peeling strength above its critical level. When the internal space is reopened, a puff of outside vapor containing B^* and N^* will rash inside to balance the pressure. At that moment the liquid droplet will again reshape and accelerate itself, resulting in a sudden change of growth rate. At the same time, this abrupt turning period is dutifully achieved in solid form of internal structures of wave-like, the knot of bamboo-like and the chain shell of bubble-chain. The characteristic growth rates for the two categories of BN nanotubes can be expressed as smooth and abrupt, respectively. A smooth rate is for cylinder (Fig. 3d), while a periodically, abruptly changing rate for bamboo-like (Fig. 3e) and wave-like and bubble-chain.

Insights into the morphology change of individual BN nanotubes from the initial to the final state are the key point for understanding growth scenarios. It is well-known that the open

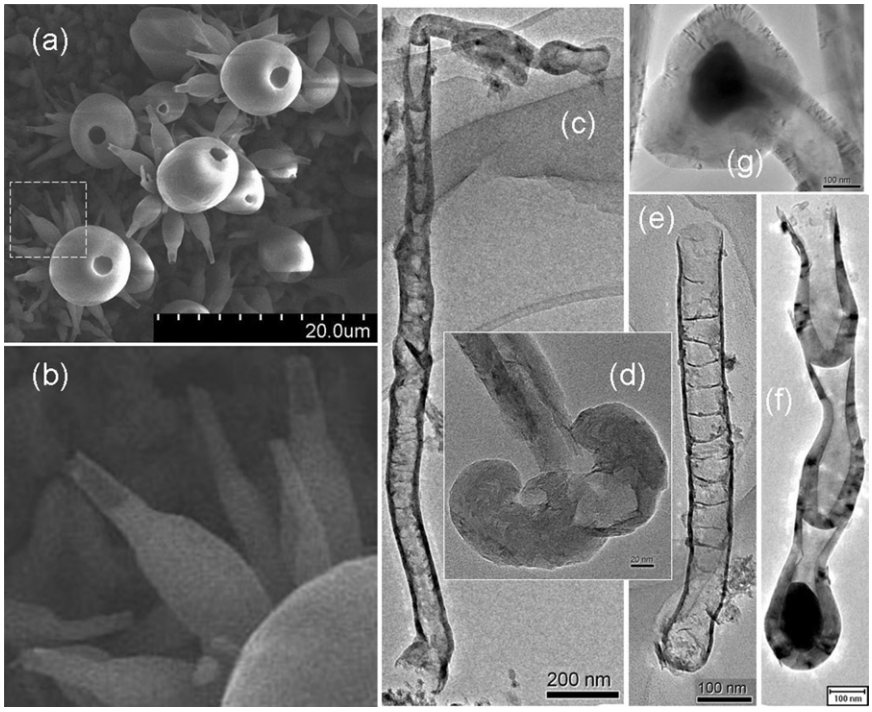

Fig. 4. SEM (a, b) and TEM (c–g) images of the open and closed ends of the as-synthesized BN nanotubes. Type and scale bar: (a) initial growth stage of cylinder, 20 μm, (b) larger magnification of partial a, (c) metamorphic BN nanotube, 200 nm, (d) typical root base, 20 nm, (e) wave-like, 100 nm, (f) bubble-chain with a encapsulated catalyst droplet, 200 nm and (g) tip with a encapsulated catalyst droplet, 100 nm.

ends of any types of BN nanotubes can be obtained when the tip catalyst and the root base are removed away from the nanotubes. Fig. 4 is the SEM (a, b) and TEM (c–g) images of the open and closed ends of the as-synthesized BN nanotubes. Fig. 4a and b displays the base growth model at the initial growth stage of cylinder BN nanotubes. The images were recorded by observing the initially annealed precursor particles using SEM. We can see that the catalyst drops were solidified in the premature nanotubes and adhered onto the base support MgO. Both the small bottles and the large jugs were nanotube embryos and all had initial open tips. These solidified embryos harbored different sizes of catalyst drops and can be grown into fully developed cylinder type of BN nanotubes of different diameters in the later annealing stage. The diameters of BN nanotubes evidently had strong correlation with the initial sizes of in-situ formed catalyst droplets. When the nanotubes were fully grown and were removed from the base, cylinder type BN nanotubes with two open ends can be obtained as shown in Fig. 1a1.

Fig. 4c shows a metamorphic BN nanotube grown by the based tip growth model after it was freed off both base and tip catalyst. This abnormal nanotube started firstly with cylinder, then wave-like, and swiftly transformed from bamboo-like to bubble-chain. Its root is obviously wide open, while the tip hole is very narrow. Fig. 4d shows a typical root after the metal catalyst has been removed completely either by washing with acid solution or by drawing up to the tip. The irregular open feature of the BN root indicates the base, base-tip or based tip growth mechanism to form a cylinder BN nanotube.

Fig. 4e and f shows the tip or base growth model of a wave-like and a bubble-chain after the growing point of catalyst particles have been removed. Unlike the base catalyst that remains stationary, tip catalyst droplets keep going during the growth process. The encapsulated catalyst particle trapped in the bubble-chain (Fig. 4f) came from partially breaking-up of initial catalyst drop and left behind. This phenomenon sometimes can periodically occur and even form a special structured BN nanotube as previously reported by Chen et al. [14]. On the other hand, the growth of BN nanotubes will cease when BN layers completely wrap outside surface of the tip droplets as shown in Fig. 4g, and the catalyst droplet will be difficult to remove by washing with hydrochloric acid.

The configuration, chirality and wall thickness are also closely associated with three-dimensional movement of catalyst droplets. Fig. 5 shows some selected SEM and TEM images of the four types of BN nanotubes with different shape, chirality and wall thickness. Fig. 5a is an unusual picture taken at the initial growth stage of the cylinder BN nanotubes by the base growth model. Three nanotube embryos grew out of the BN nanocones. In other words, the nanocones are connected with the cylinder BN nanotube embryos. The nanocones were left behind as the bases of the cylinder nanotube embryos after the division and secession of the initial droplets. Fig. 5b archived an irregular movement trace of a catalyst drop that formed a bend wave-like BN nanotube. Fig. 5c is a record of a catalyst drop flying far forth to form a long bamboo-like BN nanotube by based tip growth model, but the upside coiled shape was later formed, not representing the original movement of the liquid drop. The thick-walled bamboo BN nanotube (Fig. 5d) has a spring-like configuration of right-handed helicity. It reveals the movement history of a liquid drop going forward spirally. The irregularly grown bubble-chain BN nanotube (Fig. 5e) was the footprint of a catalyst drop staggering upward with different paces.

Small sized droplets freely flying with high velocity usually produce cylinder type of single-walled, double-walled [9] or few-walled BN nanotubes by tip growth model, like most of the BN nanotubes synthesized by physical method, but previous report by Arenal et al. [34] described it as a root-growth mechanism. In fact the so-called root has the same meaning of tip in their paraphrase. Thin BN nanotubes less than 5 nm in diameter with single and few walls were very rare in the as-synthesized BN nanotubes, but fine nanotubes appeared at it happens in Fig. 5c and d. Small amount of thick-walled BN

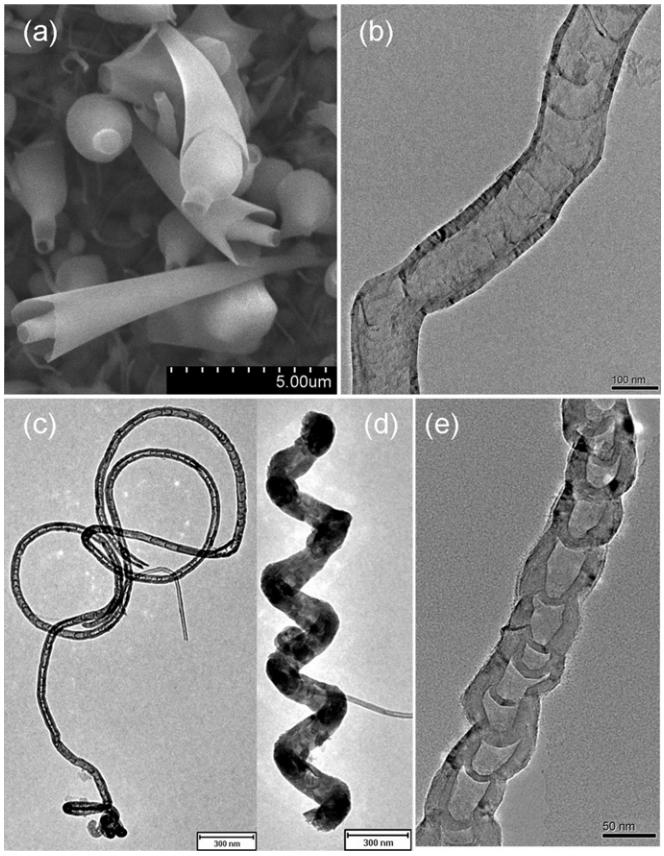

Fig. 5. Selected SEM (a) and TEM (b–e) images of the as-synthesized BN nanotubes. Type and scale bar: (a) cylinder at initial growth stage, 5 μm, (b) wave-like, 100 nm, (c, d) bamboo-likes, 300 nm and (e) bubble-chain, 50 nm.

nanotubes, like the bamboo-like BN nanotubes in Fig. 5d, were also found in the as-synthesized samples. The thick-walls may come from originally thinner BN nanotubes by consequential increment of outside BN layers through the vapor–solid (VS) growth mechanism.

We have reported the porous precursor plays a key role in bulk synthesis of BN nanotubes in Ref. [35]. The porous precursors prepared by SHS method can be low-cost raw materials that can control the loading and distribution of boron source and metal catalyst for tuning the growth rate to synthesize different types of BN nanotubes. The key point of controllable synthesis of BN nanotubes situates in the growth rates of individual BN nanotubes, because the structure of BN nanotubes is grown in a bottom-up self-assembly way. Well-designed precursors with uniform pore structure and highly dispersed composition are very significant for large batch and selective production of BN nanotubes. We also suggest a mechanism of large batch annealing of porous precursors for selective synthesis of BN nanotubes and propose the reaction processes.

4. Conclusions

In summary, four types of BN nanotubes with high yields each about 1 kg were produced with high selectivity by large batch annealing of porous precursors in flowing NH_3 and NH_3/H_2 atmosphere at temperature ranging from 1000 to 1200 °C in a vertical furnace. Characterization by SEM, FSEM, TEM, HRTEM, XRD, Raman and FTIR spectroscopy indicates the BN nanotubes have a well-crystallized hexagonal phase. The as-synthesized four types of BN nanotubes, including cylinder, wave-like, bamboo-like and bubble-chain, display different structures.

Three growth models are proposed based on the theory of catalytic VLS growth mechanism. Relevant growth rates of BN nanotubes and movement features of catalyst droplets are defined for growth scenarios and different characteristics of the as-synthesized BN nanotubes. The configuration, chirality and wall thickness are also closely associated with three-dimensional movement of catalyst droplets.

The selectivity of BN nanotubes was found to be approximately 80–95 %. Chemical reaction mechanism during the annealing of porous precursors was also discussed. The porous precursor prepared by SHS method played a key role in controlled synthesis of different types of BN nanotubes. Both stable porosity and compositional uniformity of the precursors were significant for large batch synthesis of BN nanotubes. We hope this work is helpful for popularization and application of the BN nanotubes.

References

[1] N.G. Chopra, R.J. Luyken, K. Cherrey, V.H. Crespi, M.L. Cohen, S.G. Louie, A. Zettl, Science 269 (1995) 966–967.
[2] J.S. Wang, C.H. Lee, Y.K. Yap, Nanoscale 2 (2010) 2028–2034.
[3] D. Golberg, Y. Bando, Y. Huang, T. Terao, M. Mitome, C.C. Tang, C.Y. Zhi, ACS Nano 4 (2010) 2979–2993.
[4] R.S. Wagner, W.C. Ellis, Appl. Phys. Lett. 4 (1964) 89–90.
[5] J.S. Wang, V.K. Kayastha, Y.K. Yap, Z.Y. Fan, J.G. Lu, Z.W. Pan, I.N. Ivanov, A.A. Puretzky, D.B. Geohegan, Nano Lett. 5 (2005) 2528–2532.
[6] L. Guo, R.N. Singh, Physica E 41 (2009) 448–453.
[7] C.Y. Su, Z.Y. Juang, K.F. Chen, B.M. Cheng, F.R. Chen, K.C. Leou, C.H. Tsai, J. Phys. Chem. C 113 (2009) 14681–14688.
[8] O.R. Lourie, C.R. Jones, B.M. Bartlett, P.C. Gibbons, R.S. Ruoff, W.E. Buhro, Chem. Mater. 12 (2000) 1808–1810.
[9] M.J. Kim, S. Chatterjee, S.M. Kim, E.A. Stach, M.G. Bradley, M.J. Pender, L.G. Sneddon, B. Maruyama, Nano Lett. 8 (2008) 3298–3302.
[10] P.L. Kang, F.F. Yang, Mater. Chem. Phys. 107 (2008) 115–121.
[11] C.C. Tang, M.L. de la Chapelle, P. Li, Y.M. Liu, H.Y. Dang, S.S. Fan, Chem. Phys. Lett. 342 (2001) 492–496.
[12] N. Koi, T. Oku, M. Nishijima, Solid State Commun. 136 (2005) 342–345.
[13] J. Zhang, C.J. Lu, Z.Q. Li, Chin. J. Chem. Phys 18 (2005) 113–116.
[14] Z.G. Chen, J. Zou, F. Li, G. Liu, D.M. Tang, D. Li, C. Liu, X.L. Ma, H.M. Cheng, G.Q. Lu, Z.D. Zhang, Adv. Funct. Mater. 17 (2007) 33713376.
[15] H. Tokoro, S. Fujii, T. Oku, Mater. Chem. Phys. 114 (2009) 204–212.
[16] Z.W. Gan, X.X. Ding, Z.X. Huang, X.T. Huang, C. Cheng, C. Tang, S.R. Qi, Appl. Phys. A 81 (2005) 527–529.
[17] C.H. Lee, M. Xie, V. Kayastha, J.S. Wang, Y.K. Yap, Chem. Mater. 22 (2010) 1782–1787.
[18] G. Wen, T. Zhang, X.X. Huang, B. Zhong, X.D. Zhang, H.M. Yu, Scripta Mater. 62 (2010) 25–28.
[19] K.P. Loh, M. Lin, M. Yeadon, C. Boothroyd, Z. Hu, Chem. Phys. Lett. 387 (2004) 40–46.
[20] J.J. Fu, Y.N. Lu, H. Xu, K.F. Huo, X.Z. Wang, L. Li, Z. Hu, Y. Chen, Nanotechnology 15 (2004) 727–730.
[21] Y.L. Li, B.Q. Cai, J.X. Zhang, Chin. J. Mater. Eng 10 (2008) 85–87.
[22] J. Zhang, Z.Q. Li, J. Xu, Chinese J. Mater. Sci. Technol 21 (2005) 128–130.
[23] S.D. Yuan, X.X. Ding, Z.X. Huang, X.T. Huang, Z.W. Gan, C.C. Tang, S.R. Qi, J. Cryst. Growth 256 (2003) 67–72.
[24] Y. Chen, J.F. Gerald, J.S. Williams, P. Willis, J. Metastab. Nanocryst 2 (1999) 173–178.
[25] S.Y. Bae, H.W. Seo, J. Park, Y.S. Choi, J.C. Park, S.Y. Lee, Chem. Phys. Lett. 374 (2003) 534–541.
[26] F.Q. Ji, C.B. Cao, H. Xu, Z.G. Yang, Chinese J. Mater. Eng 3 (2006) 389–393.
[27] Y.J. Li, J.E. Zhou, K. Zhao, S. Tung, E. Schneider, Mater. Lett. 63 (2009) 1733–1736.
[28] L.H. Li, Y. Chen, A.M. Glushenkov, Nanotechnology 21 (2010) 5105601 21 (2010) 5.
[29] Y. Chen, L.T. Chadderton, J. FitzGerald, J.S. Williams, Appl. Phys. Lett. 74 (1999) 960–962.
[30] J.J. Velazquez-Salazar, E. Munoz-Sandoval, J.M. Romo-Herrera, F. Lupo, M. Ruhle, H. Terrones, M. Terrones, Chem. Phys. Lett. 416 (2005) 342–348.
[31] R. Ma, Y. Bando, T. Sato, Chem. Phys. Lett. 337 (2001) 61–64.
[32] L.T. Chadderton, Y. Chen, J. Cryst. Growth 240 (2002) 164–169.
[33] S. Helveg, C. Lopez-Cartes, J. Sehested, P.L. Hansen, B.S. Clausen, J.R. Rostrup-Nielsen, F. Abild-Pedersen, J.L. Norskov, Nature 427 (2004) 426–429.
[34] R. Arenal, O. Stephan, J.L. Cochon, A. Loiseau, J. Am. Chem. Soc. 129 (2007) 16183–16189.
[35] L.P. Zhang, J.L. Wang, Y.L. Gu, G.W. Zhao, Q.L. Qian, J. Li, X.Y. Pan, Z.H. Zhang., J. Solid State Chem. 184 (2011) 633–636.